Relativistic Zel'dovich approximation in a spherically symmetric model

Masaaki Morita

Department of Physics, Tokyo Institute of Technology, Oh-Okayama, Meguro-ku, Tokyo 152, Japan

Kouji Nakamura

Advanced Science Research Center, Japan Atomic Energy Research Institute, Tokai, Naka, Ibaraki 319-11, Japan

Masumi Kasai

Department of Physics, Hirosaki University, Bunkyo-cho, Hirosaki 036, Japan

We compare relativistic approximation methods, which describe gravitational instability in the expanding universe, in a spherically symmetric model. Linear perturbation theory, second-order perturbation theory, the relativistic Zel'dovich approximation, and the relativistic post-Zel'dovich approximation are considered and compared with the Lemaître-Tolman-Bondi solution in order to examine the accuracy of these approximations. We consider some cases of inhomogeneous matter distribution while the homogeneous top-hat model has been usually taken in the previous Newtonian works. It is found that the Zel'dovich-type approximations are generally more accurate than the conventional perturbation theories in the weakly nonlinear regime. The applicable range of the Zel'dovich-type approximations is also discussed. [S0556-2821(98)04010-7]

PACS number(s): 98.80.Hw, 04.25.Nx

I. INTRODUCTION

Structure formation in the universe is an important subject of research in cosmology. A standard view of the structure formation is that density fluctuations with small amplitudes in the early universe have grown to be a variety of cosmic structures due to gravitational instability. The growth of the density fluctuations has been thoroughly investigated by linear perturbation theory of the Friedmann-Lemaître-Robertson-Walker (FLRW) universe within both the Newtonian theory and general relativity [1]. Relativistic linear perturbation theory was first derived by Lifshitz [2]. Such relativistic treatments are indispensable when we consider large-scale fluctuations. In his theory, however, there remains a gauge problem that unphysical perturbations are included in the solutions. This problem was carefully studied later by Press and Vishniac [3]. Also developed was the gauge-invariant formulation [4], which gives a conceptually straightforward way for dealing with cosmological perturbation.

It is true that the linear theories play an important role in the study of gravitational instability, but they are valid only in the region where density contrast $\delta \equiv (\rho - \rho_b)/\rho_b$ is much smaller than unity. (ρ is energy density of the perturbed FLRW universe and ρ_b is that of the background FLRW universe.) As δ grows to be comparable to unity, nonlinear effects become essential and we need some kind of nonlinear approximation. Tomita [5] developed second-order perturbation theory by extending Lifshitz's work to study the nonlinear effect of gravitational instability for the matter-dominated universe. His approach, however, still depends on the assumption of δ being small. An approximation scheme without the assumption was proposed by Zel'dovich [6] within the Newtonian framework. This scheme is known as the Zel'dovich approximation, which is now widely applied to the problems of large-scale structure formation. It has

been shown that the Zel'dovich approximation can be regarded as a subclass of the first-order solutions in Lagrangian perturbation theory [7]. Then higher-order extension of the Zel'dovich approximation, say, the post-Zel'dovich approximation (and post-post-Zel'dovich approximation and so on), is straightforwardly derived via the higher-order Lagrangian approach [8–10]. Relativistic versions of the Zel'dovich approximation have also been studied for the last few years by several authors [11–14]. Here we will focus on our tetrad-based approach, whose correspondence to the original Zel'dovich approximation is made clear in Ref. [12] and extension to second order is presented in Ref. [13].

One of the remarkably advantageous points of the Zel'dovich-type approximations, both the original Newtonian one and the relativistic version, is that they include exact solutions when the deviation from the background FLRW universe is locally one dimensional. These exact solutions are known as Zel'dovich solutions [6,15] in the Newtonian case and (some class of) Szekeres solutions [16,17] in the general relativistic case, respectively. For this reason, the Zel'dovich-type approximations are presumably accurate in description of nearly one-dimensional collapse. It is not clear, however, whether they also give high accuracy in the case of non-one-dimensional collapse. In the Newtonian framework, it has been investigated by using spherical models: The so-called top-hat collapse model [18], the top-hat void model [19], and some more general cases [10]. (See also Ref. [20] for review.) In addition, there is also a recent work [21] in which homogeneous spheroidal models are considered. An interesting implication is obtained in it: As the deviation of the models from the spherical symmetry becomes larger, the accuracy of the Zel'dovich-type approximations increases while the conventional (Eulerian) approximations have the opposite tendency. It indicates that the Zel'dovich-type approximations may be the least accurate in the exactly spherical case. Then, considering the spherical

case may tell us the lowest accuracy of the Zel'dovich-type approximations.

In general relativity, an exact solution of the spherically symmetric dust model is known as the Lemaître-Tolman-Bondi (LTB) solution [22]. It is, therefore, of interest to test the Zel'dovich-type approximations with the exact solutions to examine accuracy of the approximations. It is also instructive to clarify the differences between conventional perturbation theories and Zel'dovich-type approximations by imposing spherical symmetry and comparing them with the exact solutions.

In this paper, we compare relativistic approximations such as linear perturbation theory by Lifshitz [2], second-order perturbation theory by Tomita [5], the relativistic Zel'dovich approximation by Kasai [12], and the relativistic post-Zel'dovich approximation by Russ *et al.* [13] with the LTB solution. We consider some initial conditions which have an inhomogeneous matter distribution, not a homogeneous one similar to the top-hat model adopted in the Newtonian works. It will be shown that the Zel'dovich-type approximations are more useful than the conventional ones in the quasinonlinear regime in each case.

The plan of this paper is as follows. In the next section, we summarize the relativistic perturbation theories mentioned above. In Sec. III, the LTB solution is introduced and the relation to the relativistic perturbation theories is considered. The main results of this paper are shown in the Sec. IV. Section V contains a summary of our results and discussions.

Throughout this paper, units are chosen so that $c=1$. Indices $\mu, \nu, \ldots$, run from 0 to 3 and $i,j, \ldots$, run from 1 to 3.

II. RELATIVISTIC PERTURBATION THEORIES

In this section, we summarize general relativistic perturbation theories which describe gravitational instability in the matter-dominated FLRW universe. We assume that the background is the Einstein–de Sitter spacetime, whose line element is

$$ds^2 = -dt^2 + a^2(t)(dR^2 + R^2 d\theta^2 + R^2 \sin^2\theta d\phi^2)$$
$$\equiv -dt^2 + a^2(t)k_{ij}dx^i dx^j, \qquad (2.1)$$

where $a(t)=t^{2/3}$ is the scale factor. The background four-velocity and energy density of the matter are $u_b^\mu=(1,0,0,0)$ and $\rho_b=1/(6\pi Gt^2)$, respectively. Density contrast δ shown later is defined as $\delta\equiv(\rho-\rho_b)/\rho_b$, where ρ is energy density of the perturbed FLRW universe.

A. Conventional linear and second-order theories

Lifshitz [2] pioneered the linear perturbation of the FLRW universe in the synchronous gauge

$$ds^2 = -dt^2 + g_{ij}dx^i dx^j. \qquad (2.2)$$

In his theory, the scalar-mode solutions for pressureless matter (dust) are

$$\gamma_{ij} \equiv a^{-2}g_{ij} = \left(1+\tfrac{20}{9}\Psi\right)k_{ij} + 2t^{2/3}\Psi_{|ij} + 2t^{-1}\Phi_{|ij},$$
$$u^i_{(1)}=0, \qquad (2.3)$$
$$\delta_{(1)} = -t^{2/3}\Psi^{|k}_{|k} - t^{-1}\Phi^{|k}_{|k},$$

where $\Psi=\Psi(\boldsymbol{x})$ and $\Phi=\Phi(\boldsymbol{x})$ are spatial arbitrary functions of first-order smallness, $|$ denotes the covariant derivative associated with the background three-metric k_{ij}, and u^i represents spatial component of the four-velocity of the matter. The subscript (1) denotes the first-order perturbation quantity. We will not consider the contribution of the decaying mode, which is proportional to t^{-1}, later on.

Tomita [5] developed a second-order perturbation theory by extending Lifshitz's work. He obtained the following second-order perturbative solutions from the first-order scalar mode solutions

$$\gamma_{ij} = \left(1 + \tfrac{20}{9}\Psi + \tfrac{100}{81}\Psi^2\right)k_{ij}$$
$$+ t^{2/3}\left(2\Psi_{|ij} - \tfrac{40}{9}\Psi_{|i}\Psi_{|j} - \tfrac{20}{9}\Psi\Psi_{|ij} + \tfrac{10}{9}\Psi^{|k}\Psi_{|k}k_{ij}\right)$$
$$+ \tfrac{1}{7}t^{4/3}\{19\Psi_{|ik}\Psi^{|k}_{|j} - 12\Psi^{|k}_{|k}\Psi_{|ij}$$
$$+ 3[(\Psi^{|k}_{|k})^2 - \Psi^{|k}_{|\ell}\Psi^{|\ell}_{|k}]k_{ij}\},$$
$$u^i_{(1)}=0, \qquad u^i_{(2)}=0, \qquad (2.4)$$
$$\delta_{(1)} + \delta_{(2)} = -t^{2/3}\Psi^{|k}_{|k} + \tfrac{5}{9}t^{2/3}(\Psi^{|k}\Psi_{|k} + 6\Psi\Psi^{|k}_{|k})$$
$$+ \tfrac{1}{7}t^{4/3}[5(\Psi^{|k}_{|k})^2 + 2\Psi^{|k}_{|\ell}\Psi^{|\ell}_{|k}].$$

The subscript (2) represents the second-order perturbation. Here we neglected the second-order tensor mode, which is induced by the first-order scalar mode and does not appear in the spherical case.

B. Zel'dovich-type approximations in general relativity

In this subsection, we review a relativistic version of the Zel'dovich approximation developed by us [12,13]. (Concerning the relationship to the Newtonian Zel'dovich approximation and the details, see Ref. [12], in particular, Sec. III C.) The irrotational dust model is assumed and then we can take the comoving synchronous coordinate

$$ds^2 = -dt^2 + g_{ij}dx^i dx^j \qquad (2.5)$$

with the four-velocity $u^\mu=(1,0,0,0)$. Thanks to this choice of the gauge, the energy equation $u_\mu T^{\mu\nu}_{;\nu}=0$ with $T^{\mu\nu}=\text{diag}[\rho,0,0,0]$, which becomes

$$\dot{\rho} + \rho K^i_i = 0 \qquad (2.6)$$

is formally solved in the form

$$\rho = \rho(t_{\text{in}},\boldsymbol{x})\frac{\sqrt{\det[g_{ij}(t_{\text{in}},\boldsymbol{x})]}}{\sqrt{\det[g_{ij}(t,\boldsymbol{x})]}}. \qquad (2.7)$$

Here the overdot denotes $\partial/\partial t$, and K^i_j is the extrinsic curvature, whose expression in the present gauge is $K^i_j = \tfrac{1}{2}g^{ik}\dot{g}_{jk}$. Introducing the triad

$$g_{ij} = a^2(t)\delta_{(k)(\ell)}e_i^{(k)}e_j^{(\ell)}, \tag{2.8}$$

Eq. (2.7) is rewritten as

$$\rho = \rho_b \frac{\det[e_i^{(\ell)}(t_{\rm in}, \boldsymbol{x})]}{\det[e_i^{(\ell)}(t, \boldsymbol{x})]}. \tag{2.9}$$

We obtain perturbative solutions for the triad $e_i^{(\ell)}$ regardless of the energy density ρ up to second order in the following form [13]:

$$e_i^{(\ell)} = k_i^{(\ell)} + E_i^{(\ell)} + \varepsilon_i^{(\ell)}, \tag{2.10}$$

where $k_i^{(\ell)}$ is the background triad defined by $k_{ij} = \delta_{(k)(\ell)}k_i^{(k)}k_j^{(\ell)}$, and $E_i^{(\ell)}$ and $\varepsilon_i^{(\ell)}$ are the first-order and the second-order solutions given by

$$E_i^{(\ell)} = k_j^{(\ell)}\left(\frac{10}{9}\Psi\,\delta^j{}_i + t^{2/3}\Psi^{|j}{}_{|i}\right),$$

$$\varepsilon_i^{(\ell)} = k_j^{(\ell)}(t^{2/3}\psi^j{}_i + t^{4/3}\varphi^j{}_i). \tag{2.11}$$

Here $\Psi = \Psi(\boldsymbol{x})$ is the same function as the one used in Eqs. (2.3) and (2.4), and $\psi^i{}_j = \psi^i{}_j(\boldsymbol{x})$ and $\varphi^i{}_j = \varphi^i{}_j(\boldsymbol{x})$ are quadratic quantities of Ψ, written as

$$\psi^i{}_j = \frac{5}{9}\Psi^{|k}{}_{|k}\delta^i{}_j - \frac{20}{9}(\Psi\Psi^{|i}{}_{|j} + \Psi^{|i}\Psi_{|j}), \tag{2.12}$$

$$\varphi^i{}_j = \frac{3}{14}[(\Psi^{|k}{}_{|k})^2 - \Psi^{|k}{}_{|\ell}\Psi^{|\ell}{}_{|k}]\delta^i{}_j - \frac{6}{7}(\Psi^{|k}{}_{|k}\Psi^{|i}{}_{|j} - \Psi^{|i}{}_{|k}\Psi^{|k}{}_{|j}). \tag{2.13}$$

Note that we removed a remaining gauge freedom in the linear level to derive the above solution. (See Appendix A of Ref. [13].) And we again neglected contributions of the decaying scalar mode and the tensor mode. We find that the solution (2.10) is consistent in the metric level with Eqs. (2.3) and (2.4) [13].

Relativistic Zel'dovich and post-Zel'dovich approximations are obtained by substituting Eq. (2.10) into Eq. (2.9):

$$\delta_{\rm ZA} = \left(\det\left[\delta^i{}_j + \frac{t^{2/3}\Psi^{|i}{}_{|j}}{1 + \frac{10}{9}\Psi}\right]\right)^{-1} - 1, \tag{2.14}$$

$$\delta_{\rm PZA} = \left(\det\left[\delta^i{}_j + \frac{t^{2/3}\Psi^{|i}{}_{|j} + t^{2/3}\psi^i{}_j + t^{4/3}\varphi^i{}_j}{1 + \frac{10}{9}\Psi}\right]\right)^{-1} - 1. \tag{2.15}$$

ZA and PZA denote the Zel'dovich and the post-Zel'dovich approximations.

As was written previously, the results of the conventional linear and second-order theories are

$$\delta_{\rm lin} = -t^{2/3}\Psi^{|k}{}_{|k}, \tag{2.16}$$

$$\delta_{\rm sec} = -t^{2/3}\Psi^{|k}{}_{|k} + \frac{5}{9}t^{2/3}(\Psi^{|k}\Psi_{|k} + 6\Psi\Psi^{|k}{}_{|k})$$

$$+ \frac{1}{7}t^{4/3}[5(\Psi^{|k}{}_{|k})^2 + 2\Psi^{|k}{}_{|\ell}\Psi^{|\ell}{}_{|k}]. \tag{2.17}$$

lin and sec denote the linear and the second-order perturbation theories. Expanding Eqs. (2.14) and (2.15) under the condition $||\Psi|| \ll 1$ (where $||\Psi||$ denotes an appropriate norm of a function Ψ), Eqs. (2.16) and (2.17) can also be obtained, respectively. In this sense, ZA and PZA are extensions of lin and sec to $|\delta| \sim 1$.

III. SPHERICALLY SYMMETRIC MODEL

In this section, we consider the spherically symmetric model of gravitational instability in the FLRW universe. There exists an exact solution known as the LTB solution, which includes three arbitrary functions, in the spherically symmetric case [22]. Here we make clear the relations between the arbitrary functions included in the LTB solution and the ones which appears in the approximation methods mentioned in the Sec. II. The line element of the LTB solution is

$$ds^2 = -dt^2 + \frac{r'^2}{1 + f}dR^2 + r^2(d\theta^2 + \sin^2\theta\,d\phi^2), \tag{3.1}$$

where $(') \equiv \partial/\partial R$ and $f = f(R)$ is an arbitrary function which is related to initial velocity of dust. $r = r(t, R)$ satisfies the following differential equation:

$$\dot{r}^2 = \frac{F(R)}{r} + f(R) \tag{3.2}$$

with an arbitrary function $F(R)$, which represents initial distribution of matter. Equation (3.2) can be integrated as follows:

(i) $f > 0$:

$$r = \frac{F}{2f}(\cosh\eta - 1), \quad t - t_0(R) = \frac{F}{2f^{3/2}}(\sinh\eta - \eta), \tag{3.3}$$

(ii) $f < 0$:

$$r = \frac{F}{-2f}(1 - \cos\eta), \quad t - t_0(R) = \frac{F}{2(-f)^{3/2}}(\eta - \sin\eta), \tag{3.4}$$

(iii) $f = 0$:

$$r = \left(\frac{9F}{4}\right)^{1/3}[t - t_0(R)]^{2/3}, \tag{3.5}$$

where $t_0(R)$ is an integration constant. The above cases (i), (ii), and (iii) may be called ''open,'' ''closed,'' and ''flat,'' respectively, as in the FLRW universe. In these three cases, the density reads

$$8\pi G\rho = \frac{F'}{r'r^2}. \tag{3.6}$$

Apparently the LTB solution includes the three arbitrary functions $f(R)$, $F(R)$, and $t_0(R)$. But the dynamical degrees of freedom are actually 2 because there remains the freedom of the choice of the radial coordinate R.

The LTB solution is some extension of the FLRW solution and is often used as a model of an inhomogeneous universe (see Ref. [17] for a review), and this solution can be reduced to the FLRW solution. By choosing $f=0$ and $t_0 = 0$ (and $F = \frac{4}{9}R^3$ for convenience), we easily find that $r = a(t)R$ and the LTB solution is reduced to the spatially flat FLRW solution (2.1). Furthermore, we can represent this solution by the form of the flat FLRW solution with its perturbations and see that the arbitrary functions in the LTB solution correspond to those in linear perturbation theory. To see this, we consider a spherical linear perturbation of the spatially flat FLRW solution. Substituting

$$f=f_{(1)}, \quad t_0 = t_{0(1)}, \quad F=\frac{4}{9}R^3 + F_{(1)}, \quad r=aR+r_{(1)}, \tag{3.7}$$

into Eq. (3.2), the linearized equation for $r_{(1)}$ can be obtained, where the quantities with subscript (1) are treated as a linear perturbation. Solving this equation, we obtain

$$r_{(1)} = aR\left(\frac{3}{4}F_{(1)}R^{-3} + \frac{9}{20}t^{2/3}f_{(1)}R^{-2} + t^{-1}B\right), \tag{3.8}$$

where $B=B(R)$ is an integration constant. Actually B is related to $t_{0(1)}$ by $B=-\frac{2}{3}t_{0(1)}$. It is easily seen by choosing $f=0$ and using Eq. (3.5), which reads

$$r_{(1)} = aR\left(\frac{3}{4}F_{(1)}R^{-3} - \frac{2}{3}t^{-1}t_{0(1)}\right). \tag{3.9}$$

Then we can write the "linearized LTB metric" in terms of $f_{(1)}$, $t_{0(1)}$, and $F_{(1)}$ as follows:

$$\gamma_{RR} = 1 + \frac{3}{2}(F_{(1)}R^{-2})' - f_{(1)}$$

$$+ \frac{9}{10}t^{2/3}(f_{(1)}R^{-1})' - \frac{4}{3}t^{-1}(t_{0(1)}R)',$$

$$\gamma_{\theta\theta} = R^2\left(1 + \frac{3}{2}F_{(1)}R^{-3} + \frac{9}{10}t^{2/3}f_{(1)}R^{-2} - \frac{4}{3}t^{-1}t_{0(1)}\right). \tag{3.10}$$

On the other hand, the solution of linear theory (2.3) gives

$$\gamma_{RR} = 1 + \frac{20}{9}\Psi + 2t^{2/3}\Psi'' + 2t^{-1}\Phi'',$$

$$\gamma_{\theta\theta} = R^2\left(1 + \frac{20}{9}\Psi + 2t^{2/3}\Psi'R^{-1} + 2t^{-1}\Phi'R^{-1}\right). \tag{3.11}$$

Comparing Eqs. (3.10) and (3.11), we find the following relations:

$$F_{(1)} = \frac{40}{27}\Psi R^3, \quad f_{(1)} = \frac{20}{9}\Psi'R, \quad t_{0(1)} = -\frac{3}{2}\Phi'R^{-1}. \tag{3.12}$$

This tells us that the arbitrary functions $f(R)$ and $t_0(R)$ correspond to the growing and decaying modes, respectively, in the linear level. We choose $t_0(R)=0$ hereafter because contributions of the decaying mode are not taken into account throughout. Moreover, we know that $F_{(1)}$ and $f_{(1)}$ are related to each other by the function Ψ. This is because we eliminated a residual gauge freedom and thus fixed the gauge condition completely in the previous section. This fixing corresponds to determination of the choice of the radial coordinate R in the spherical case.

To see the relation between the LTB solution and the second-order perturbation, we introduce $f_{(2)}$, $F_{(2)}$, and $r_{(2)}$ so that

$$f = \frac{20}{9}\Psi'R + f_{(2)}, \quad F = \frac{4}{9}R^3 + \frac{40}{27}\Psi R^3 + F_{(2)},$$

$$r = aR + r_{(1)} + r_{(2)}, \tag{3.13}$$

and make calculations in the same way. Here $f_{(2)}$, $F_{(2)}$, and $r_{(2)}$ should be regarded as $O(\|\Psi\|^2)$ and $r_{(2)}$ is obtained by solving Eq. (3.2) perturbatively. Then we obtain the part of $O(\|\Psi\|^2)$ in γ_{RR} and $\gamma_{\theta\theta}$. Comparing these γ_{RR} and $\gamma_{\theta\theta}$ with the solution of the second-order theory (2.4), we find

$$F_{(2)} = \frac{400}{243}\Psi^2 R^3, \quad f_{(2)} = \frac{100}{81}(\Psi'^2 R^2 - 2\Psi\Psi'R). \tag{3.14}$$

On the other hand, the LTB solution as an exact model is obtained by choosing

$$F = \frac{4}{9}R^3 + \frac{40}{27}\Psi R^3 + \frac{400}{243}\Psi^2 R^3, \tag{3.15}$$

$$f = \frac{20}{9}\Psi'R + \frac{100}{81}(\Psi'^2 R^2 - 2\Psi\Psi'R). \tag{3.16}$$

From Eq. (3.6), the density contrast of the LTB solution reads

$$\delta_{\text{LTB}} = \frac{3}{4}\frac{t^2 F'}{r'r^2} - 1. \tag{3.17}$$

Let us turn our attention to the approximation methods. If we impose $\Psi = \Psi(R)$, Eqs. (2.16), (2.17), (2.14), and (2.15) become

$$\delta_{\mathrm{lin}} = -t^{2/3}(\Psi'' + 2\Psi'R^{-1}), \qquad (3.18)$$

$$\delta_{\mathrm{sec}} = -t^{2/3}(\Psi'' + 2\Psi'R^{-1}) + \frac{5}{9}t^{2/3}[\Psi'^2 + 6\Psi(\Psi'' + 2\Psi'R^{-1})]$$

$$+ t^{4/3}\left(\Psi''^2 + \frac{20}{7}\Psi''\Psi'R^{-1} + \frac{24}{7}\Psi'^2R^{-2}\right), \qquad (3.19)$$

$$\delta_{\mathrm{ZA}} = \left(1 + \frac{t^{2/3}\Psi'R^{-1}}{1 + \frac{10}{9}\Psi}\right)^{-2}\left(1 + \frac{t^{2/3}\Psi''}{1 + \frac{10}{9}\Psi}\right)^{-1} - 1, \qquad (3.20)$$

$$\delta_{\mathrm{PZA}} = \left(1 + {}_t^{2/3}\Psi'R^{-1} + \tfrac{5}{9}t^{2/3}(\Psi'^2 - 4\Psi\Psi'R^{-1}) - \tfrac{3}{7}\right)t^{4/3}\Psi'^2R^{-2}1 + (10/9)\Psi^{-2}$$

$$\times\left(1 + \frac{t^{2/3}\Psi'' - \tfrac{5}{9}t^{2/3}(3\Psi'^2 + 4\Psi\Psi'') - \tfrac{3}{7}t^{4/3}\Psi'R^{-1}(2\Psi'' - \Psi'R^{-1})}{1 + \frac{10}{9}\Psi}\right)^{-1} - 1. \qquad (3.21)$$

The peculiar velocity, which represents the deviation of motion of the dust shell from the Hubble expansion and is defined by $v \equiv \dot{r} - Hr$ (where $H \equiv \dot{a}/a$ is the Hubble parameter) is written as

$$v_{\mathrm{lin}} = v_{\mathrm{ZA}} = \frac{2}{3}t^{1/3}\Psi', \qquad (3.22)$$

$$v_{\mathrm{sec}} = v_{\mathrm{PZA}} = \frac{2}{3}t^{1/3}\Psi' + \frac{10}{27}t^{1/3}(\Psi'^2R - 4\Psi\Psi')$$
$$- \frac{4}{7}t\Psi'^2R^{-1}. \qquad (3.23)$$

The above expressions are similar to those in the Newtonian case, which are, for example, given in the Appendix of Ref. [10]. Note that $v_{\mathrm{lin}} = v_{\mathrm{ZA}}$ and $v_{\mathrm{sec}} = v_{\mathrm{PZA}}$ because, in the metric level, the Zel'dovich-type approximations coincide with the conventional ones.

Now the density contrast and the peculiar velocity of the LTB solution and the approximations are written in terms of only the function Ψ. The function Ψ should be determined from initial conditions so that the regularity conditions at $R = 0$, i.e., $\Psi(R=0) = 0$ and $\Psi'(R=0) = 0$ are satisfied. Then the peculiar velocity at $R = 0$ is always zero both in the LTB solution and the approximation. Moreover, if Ψ is taken so that $\Psi \propto R^2$ near $R = 0$, the peculiar velocity near $R = 0$ is proportional to R, $v \propto R$.

IV. COMPARISON OF LTB SOLUTION AND APPROXIMATIONS

Let us proceed with a comparison of the LTB solution and the approximations. As mentioned in Sec. II, δ_{ZA} and δ_{PZA} include δ_{lin} and δ_{sec}, respectively, when the density contrast is small. As for the peculiar velocity, ZA and PZA are coincident with lin and sec, respectively. Moreover, expanding the density contrast of ZA in the following form:

$$\delta_{\mathrm{ZA}} \simeq -t^{2/3}(\Psi'' + 2\Psi'R^{-1}) + \frac{10}{9}t^{2/3}\Psi(\Psi'' + 2\Psi'R^{-1})$$
$$+ t^{4/3}(\Psi''^2 + 2\Psi''\Psi'R^{-1} + 3\Psi'^2R^{-2}) + O(\|\Psi\|^3), \qquad (4.1)$$

it is found that ZA includes second-order (and higher) terms partially in the expression of the density contrast. Thus we can expect that δ_{ZA} is as accurate as δ_{sec} at late time.

In order to investigate the relative accuracy of the approximations quantitatively, we compare the LTB solution and the approximations by using some specific initial conditions. Here initial conditions can be completely fixed by giving an initial density profile $\delta_{\mathrm{in}}(R)$. For simplicity, we assume that $\delta_{\mathrm{in}}(R)$ is a first-order quantity. Then the arbitrary function Ψ is determined by the relation

$$\delta_{\mathrm{lin}}|_{t=t_{\mathrm{in}}} = -(\Psi'' + 2\Psi'R^{-1}) = \delta_{\mathrm{in}}(R) \qquad (4.2)$$

with normalization $t_{\mathrm{in}} = 1$. (t_{in} may be regarded as the decoupling time in the history of the expanding universe.) Equation (4.2) is solved to determine the function Ψ with the boundary conditions $\Psi(R=0) = 0$ and $\Psi'(R=0) = 0$.

Here we consider the following two cases:

$$\delta_{\mathrm{in}}(R) = \epsilon\left(1 + \frac{R}{R_0}\right)\exp\left(-\frac{R}{R_0}\right) \qquad (4.3)$$

and

$$\delta_{\mathrm{in}}(R) = \epsilon\left[1 + \frac{R}{R_0} - \left(\frac{R}{R_0}\right)^2\right]\exp\left(-\frac{R}{R_0}\right), \qquad (4.4)$$

where ϵ is a small constant ($|\epsilon| \ll 1$) which represents amplitude of an initial density perturbation, and R_0 is a comoving scale of the fluctuations. The former case can be regarded as smoothing out the top-hat model while in the latter case, if $\epsilon < 0$, the neighborhood of $R = 0$ is the underdense region (void) and the outside is overdense, and then the shell crossing will occur. (If $\epsilon > 0$, the latter case also shows a similar

behavior to the top-hat model, as does the former one.) For both of the cases, we can evaluate δ at the center of the fluctuations ($R=0$) from the LTB solution and the approximation methods in the following form:

$$\delta_{\text{LTB}}(R=0) = \begin{cases} \dfrac{9}{2} \dfrac{(\eta - \sin\eta)^2}{(1-\cos\eta)^3} - 1, & \text{for} \quad \epsilon > 0, \\[4mm] \dfrac{9}{2} \dfrac{(\eta - \sinh\eta)^2}{(\cosh\eta - 1)^3} - 1, & \text{for} \quad \epsilon < 0, \end{cases}$$

(4.5)

with

$$t = \begin{cases} \dfrac{9}{20} \sqrt{\dfrac{3}{5}} \epsilon^{-3/2} (\eta - \sin\eta), & \text{for} \quad \epsilon > 0, \\[4mm] \dfrac{9}{20} \sqrt{\dfrac{3}{5}} (-\epsilon)^{-3/2} (\sinh\eta - \eta), & \text{for} \quad \epsilon < 0, \end{cases}$$

and

$$\delta_{\text{lin}}(R=0) = \epsilon t^{2/3}, \tag{4.6}$$

$$\delta_{\text{sec}}(R=0) = \epsilon t^{2/3} + \frac{17}{21}\epsilon^2 t^{4/3}, \tag{4.7}$$

$$\delta_{\text{ZA}}(R=0) = \left(1 - \frac{\epsilon}{3}t^{2/3}\right)^{-3} - 1, \tag{4.8}$$

$$\delta_{\text{PZA}}(R=0) = \left(1 - \frac{\epsilon}{3}t^{2/3} - \frac{\epsilon^2}{21}t^{4/3}\right)^{-3} - 1. \tag{4.9}$$

These expressions do not depend on the details of initial density profiles. It is of essence in the calculation that $\delta_{\text{in}} \simeq \epsilon$ near $R=0$, and $\epsilon > 0$ and $\epsilon < 0$ correspond to $f < 0$ and $f > 0$ at $R=0$, respectively. The above results are described in Figs. 1 and 2, where Eqs. (4.5)–(4.9) are plotted as functions of $\delta_{\text{LTB}}(R=0)$. Figure 1, which represents the collapse case, tells us that ZA is more accurate than lin and PZA is more accurate than sec in all $\delta_{\text{LTB}}(R=0) > 0$ regions. [Figure 1 shows only the region of $0 < \delta_{\text{LTB}}(R=0) < 1$, but the tendency shown in Fig. 1 does not change in denser region $\delta_{\text{LTB}}(R=0) > 1$]. We also find that ZA becomes more accurate than sec at late time when δ_{LTB} is larger than about 0.5. This is understood by comparing Eq. (4.7) and the expanded form of Eq. (4.8):

$$\delta_{\text{ZA}}(R=0) \simeq \epsilon t^{2/3} + \frac{2}{3}\epsilon^2 t^{4/3} + O(\epsilon^3). \tag{4.10}$$

[This form is also obtained from Eq. (4.1).] We see from Eqs. (4.7) and (4.10) that δ_{ZA} is smaller than δ_{sec} at early time ($\epsilon t^{2/3} \ll 1$) due to the lack of the terms in $O(\epsilon^2)$. In this sense, δ_{ZA} is less accurate than δ_{sec} when $\epsilon t^{2/3} \ll 1$. However, due to the existence of the singularity at $\epsilon t^{2/3} = 3$ in δ_{ZA}, δ_{ZA} becomes more accurate than δ_{sec} at late time. This existence of the singularity in δ_{ZA} essentially determines the asymptotic behavior of δ_{ZA}. Indeed, the exact solution δ_{LTB} for $\epsilon > 0$ in Eq. (4.5) has a pole of order 3 at $\epsilon t^{2/3}$
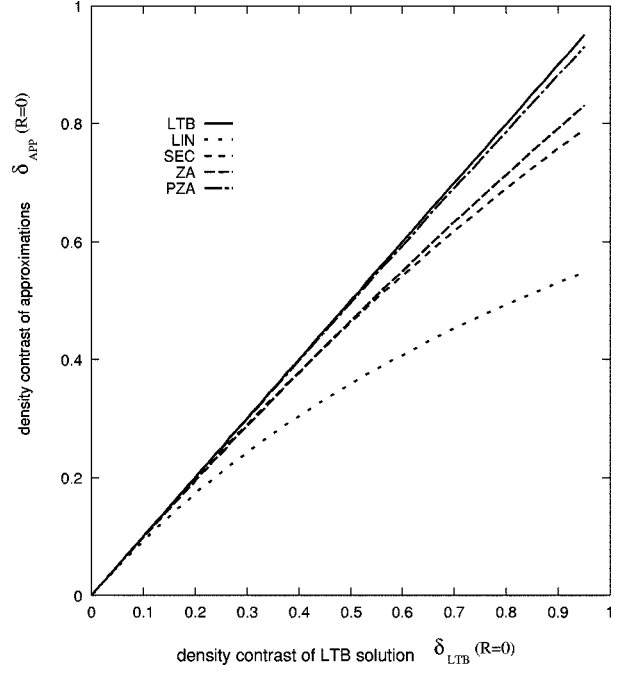

FIG. 1. Density contrast δ at $R=0$ calculated from approximation methods as a function of $\delta_{\text{LTB}}(R=0)$ for $\epsilon > 0$. $\delta_{\text{ZA}}(R=0)$ catches up with $\delta_{\text{sec}}(R=0)$ at $\delta_{\text{LTB}}(R=0) \sim 0.5$.

$= 3(3\pi/2)^{2/3}/5 \sim 1.7$ ($\eta = 2\pi$). This pole corresponds to the crunching time at $R=0$, and the singularity occurs at this time.

From Eqs. (4.5)–(4.9), we can also evaluate accuracy of the approximations quantitatively at the turnaround time $\eta = \pi$ [$\epsilon t^{2/3} = 3(9\pi^2/2)^{1/3}/10 \sim 1.1$], though it is not drawn in Fig. 1. Here the turnaround time is characterized by $\dot{r} = 0$, i.e., the maximum expansion. Physically speaking, the density fluctuation begins to collapse due to gravitational instability, overcoming the cosmic expansion at the turnaround
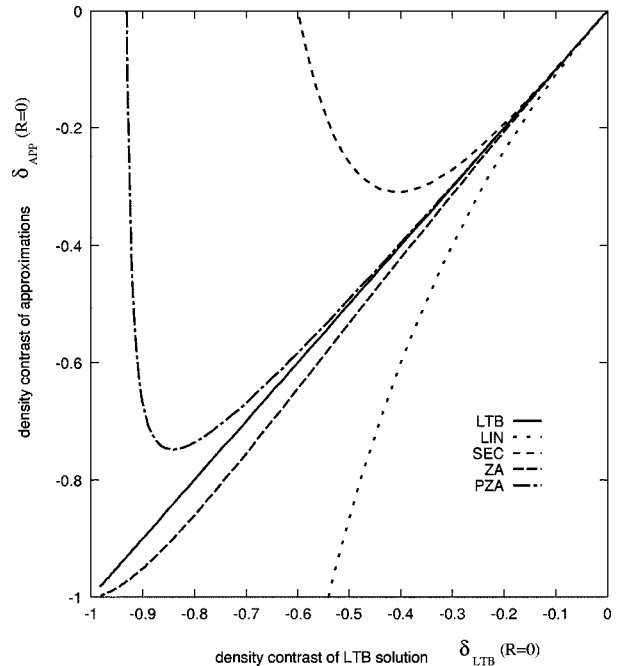

FIG. 2. Same as in Fig. 1, but for $\epsilon < 0$.

time. At the turnaround time, δ_{LTB} becomes 4.6. To this δ_{LTB}, δ_{lin}, δ_{sec}, δ_{ZA}, and δ_{PZA} grow to about 23, 43, 60, and 84%, respectively. It is natural that δ_{PZA} is more accurate than δ_{ZA} from the view point of the singularity at the crunching time. δ_{PZA} also has a pole of order 3 at $\epsilon t^{2/3} = (\sqrt{133}-7)/2 \sim 2.3$. This crunching time is nearer to the real crunching time ~ 1.7 than that of δ_{ZA}.

From Fig. 2, which denotes the void case, we find that PZA gives the best fit at early time before $\delta_{\mathrm{LTB}} \simeq -0.7$ while ZA works best at late time when δ_{LTB} is smaller than about -0.7. At late time, PZA gives bad results. It is due to difference of the signature between the first-order $(-\epsilon t^{2/3}/3 > 0)$ and the second-order $(-\epsilon^2 t^{4/3}/21 < 0)$ terms when $\epsilon < 0$. The same feature also appears in sec but at an earlier time. However, in PZA, this difference is more serious than in sec. In sec, δ_{sec} grows as $\epsilon^2 t^{4/3}/21 < 0$, while in PZA, the difference of the signature makes δ_{PZA} diverge at a finite time $\epsilon t^{2/3} = (7 + \sqrt{133})/2$. This divergence is an apparent one which is caused by the formalization of PZA. Indeed, we can easily see from Eq. (4.5) that the exact solution δ_{LTB} has no pole in $t > 0$ (i.e., there is no singularity) and approaches to -1 as $\sim t^{-1}$. Though there is no singular point in δ_{lin} except $t = \infty$, δ_{lin} takes a value smaller and smaller without limit as the time increases because there is no physics to stop this decrease of the energy density in this order. Then, only δ_{ZA} predicts the true asymptotic value of δ without growth and apparent singularities. But δ_{ZA} approaches -1 as t^{-2}. This difference is also seen in Fig. 2. In the Newtonian case, detailed discussions on the void can be seen in Ref. [19]. Our relativistic results up to now are quite similar to Newtonian ones, which are given in Refs. [10,18,19].

Figures 3(a) and 4(a) give the density contrast as a function of R/R_0 when $\epsilon = 1.0 \times 10^{-3}$ and $t = 2.0 \times 10^4$, and $\epsilon = -1.0 \times 10^{-3}$ and $t = 3.7 \times 10^4$ with the initial density profile (4.3), respectively. These two figures show that difference between the LTB solution and the approximations is the largest at $R = 0$ in the former case. Hence, it is sufficient to consider the difference at $R = 0$ when we examine the accuracy of the approximations in the former case (4.3).

We also see the evolution of the peculiar velocity with the initial density profile (4.3) in Figs. 3(b) and 4(b). Here we consider the peculiar velocity normalized by the Hubble flow Hr. It will be convenient to use it to see the deviation of the model from the FLRW universe in the metric level. For example, the normalized peculiar velocity $v/Hr = -1$ at the turnaround time. Figures 3(b) and 4(b) show the normalized peculiar velocity corresponding to Figs. 3(a) and 4(a). Although these figures show that the normalized peculiar velocity v/Hr is not zero at $R = 0$, we must note that this is due to our normalization. As mentioned in the last section, the peculiar velocity must behave as $\sim R$ near $R = 0$. On the other hand, Hr also behaves as $\sim R$ near $R = 0$. Hence our normalized peculiar velocity does not vanish at $R = 0$ due to the normalization. It is also noted that the peculiar velocity obtained from the Zel'dovich-type approximations is the same as the one obtained from the conventional approximations as mentioned in the previous section. Furthermore, we find from Figs. 3(b) and 4(b) that the deviation from the FLRW universe is maximum near $R = 0$ for the initial profile (4.3). This also shows that it is sufficient to consider the
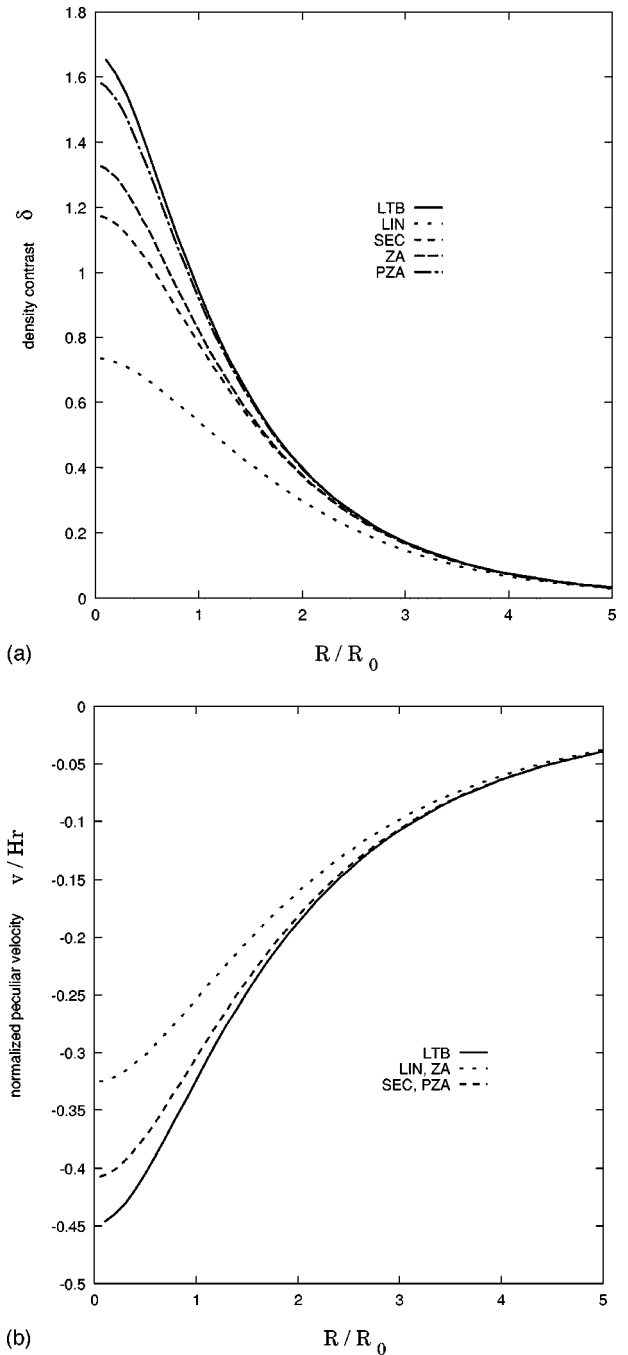

FIG. 3. (a) Profile of density contrast when $\delta_{\mathrm{in}} = \epsilon(1 + R/R_0)\exp(-R/R_0)$ and $t = 2.0 \times 10^4$ with $\epsilon = 1.0 \times 10^{-3}$. (b) Profile of normalized peculiar velocity corresponding to (a).

difference at $R = 0$ when we examine the accuracy of the approximations in the former case (4.3), as mentioned above.

On the other hand, for the initial density profile given by Eq. (4.4), it cannot be said that the largest deviation of the approximations from the LTB solution occurs at $R = 0$. Figures 5(a) and 6(a) are for this initial profile when $\epsilon = -1.0 \times 10^{-3}$ and $t = 2.0 \times 10^5$, and $\epsilon = -1.0 \times 10^{-3}$ and $t = 3.0 \times 10^5$, respectively. For this initial density profile, the shell-crossing singularity will occur. The tendency of the occurring of shell crossing can be seen from the peculiar velocity in Figs. 5(b) and 6(b), where the profile of the normalized peculiar velocities for this case are drawn. In Figures 5(b)
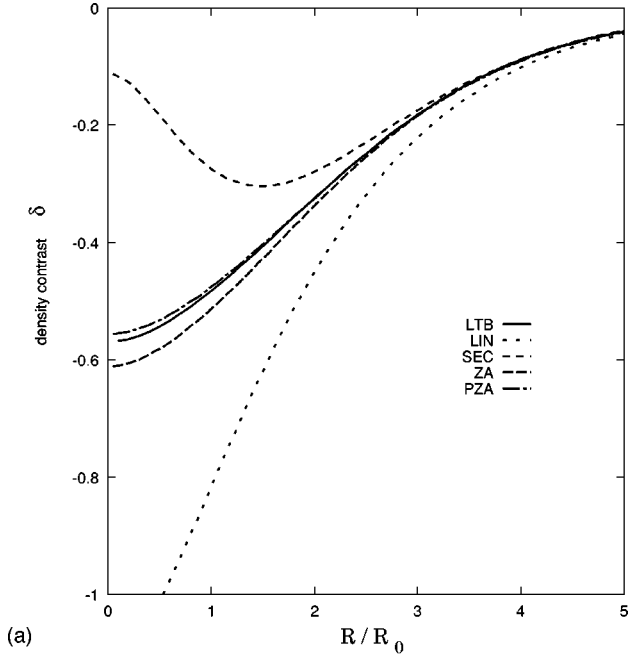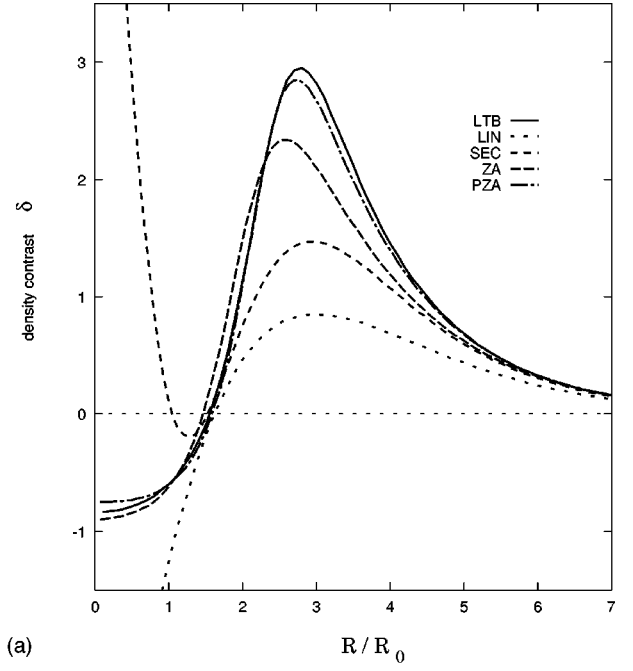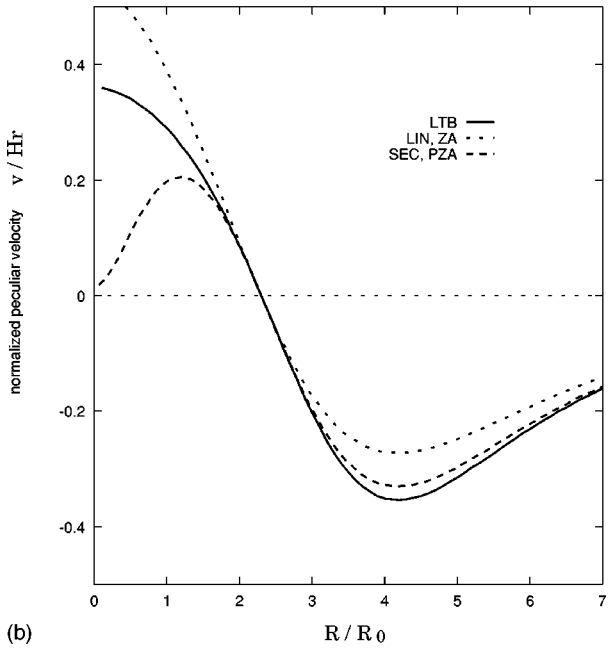
(a)
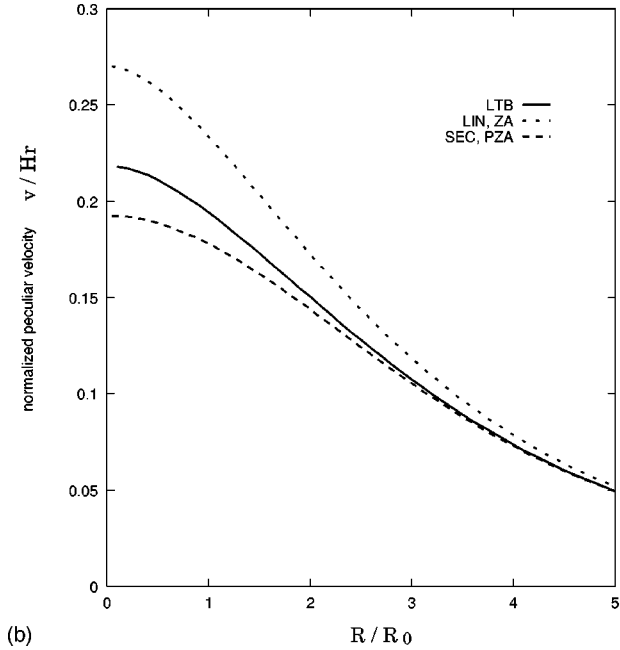
(b)

FIG. 4. (a) Same as in Fig. 3(a), but for the void case. We choose $\epsilon = -1.0 \times 10^{-3}$ and $t = 3.7 \times 10^4$. (b) Profile of normalized peculiar velocity corresponding to (a).

(a)

(b)

FIG. 5. (a) Profile of density contrast when $\delta_{in} = \epsilon [1 + R/R_0 - (R/R_0)^2] \exp(-R/R_0)$ and $t = 2.0 \times 10^5$ with $\epsilon = -1.0 \times 10^{-3}$. (b) Profile of normalized peculiar velocity corresponding to (a).

and 6(b), there exists a $v = 0$ point at $R/R_0 \sim 2.5$. This point, which is denoted by $R = R_c \neq 0$ hereafter, is a boundary where the universe is locally "open" ($f > 0$) and "closed" ($f < 0$), and then $f = 0$ at the point. The peculiar velocity in the void region $R < R_c$ is positive, while that in the closed region $R > R_c$ is negative. Then we can expect that the shell crossing of the dust matter will form at $R = R_c$ within a finite time.

Indeed, one can see from Eqs. (3.2) and (3.5) that the shell crossing, which is characterized by a finite radius at which r' vanishes [23], will occur at the radius $R = R_c$. From Eq. (3.5), which is the solution when $f = 0$, we know

$$r_c = \left(\frac{9 F_c}{4} \right)^{1/3} t^{2/3}. \qquad (4.11)$$

(Subscript c denotes value at $R = R_c$.) Differentiating Eq. (3.2) with respect to R and using Eq. (4.11), we obtain the equation for r'_c. Integrating this equation, one finds

$$r'_c = \frac{3 F'_c}{4} \left(\frac{4}{9 F_c} \right)^{2/3} t^{2/3} + \frac{3}{5} \left(\frac{4}{9 F_c} \right)^{1/3} f'_c t^{4/3} + C t^{-1/3}, \qquad (4.12)$$
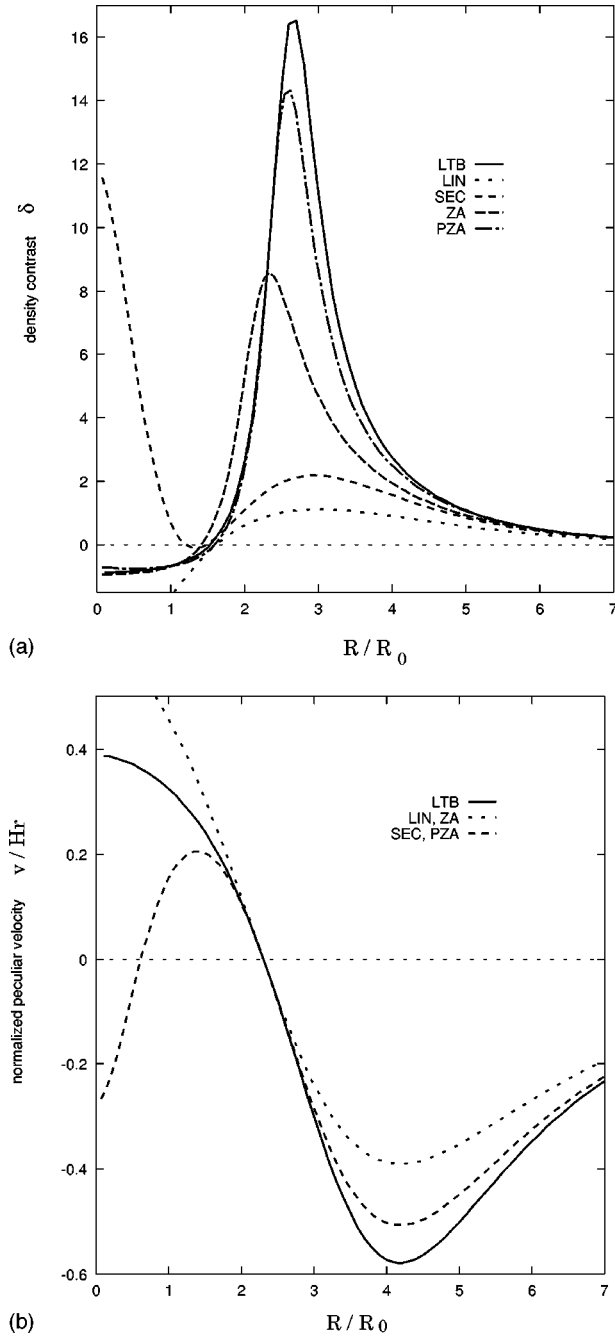
FIG. 6. (a) Same as in Fig. 5(a), but for $t=3.0\times10^5$. (b) Profile of normalized peculiar velocity corresponding to (a).

where C is an integration constant and is not essential in our argument. Here, r' must be positive initially if r is a monotonically increasing function of R, which it is in our case. This means that the first term (cooperate with the third term) in Eq. (4.12) must dominate on the initial surface. However, since $f'_c<0$ at $R=R_c$, r'_c must vanish within a finite time. Hence, at $R=R_c$, the shell-crossing singularity will occur. (More generic arguments about the occurrence of shell-crossing singularity can be seen in Ref. [23] and the shell-crossing may occur in the region $f<0$ at first).

It should be noted that in Figs. 5(a) and 6(a), δ_{ZA} and δ_{PZA} take the same value as that of the LTB solution at $R=R_c$ where the shell crossing will occur. Then we must say that these figures show that the Zel'dovich-type approxima-

tions are not necessarily inaccurate even when the shell crossing is occurring. Let us consider the reason here. In fact, the deviation from the background Hubble expansion is locally one dimensional at the point. The definition of ''locally one-dimensional deviation'' we adopt here is that two of the eigenvalues of the peculiar deformation tensor $V^i{}_j\equiv K^i{}_j -H\delta^i{}_j=\frac{1}{2}\gamma^{ik}\dot\gamma_{jk}$ are zero [24]. According to the definition, let us show the local one dimensionality at $R=R_c\neq0$. From Eqs. (3.1) and (4.11),

$$V^R{}_R|_{R=R_c}=\frac{\dot r'_c}{r'_c}-\frac{\dot a}{a}\neq0,$$

$$V^\theta{}_\theta|_{R=R_c}=V^\phi{}_\phi|_{R=R_c}=\frac{\dot r_c}{r_c}-\frac{\dot a}{a}=0;\quad v_{LTB}|_{R=R_c}=0.$$
(4.13)

Since $V^i{}_j$ is diagonal in the spherical case, this means that the deviation at $R=R_c$ is locally one dimensional. It is known that the Zel'dovich-type approximations become exact when the deviation is locally one dimensional [12,24]. In this argument, the origin $R=0$ must be excluded because all components of the peculiar velocity vanish at the origin. Thus we can lead a significant consequence that, at the points where $f=0$, the Zel'dovich-type approximations coincide with the exact LTB solution, i.e.,

$$\delta_{LTB}=\delta_{ZA}=\delta_{PZA}\quad\text{and}\quad v_{LTB}=v_{ZA}=v_{PZA}=0.$$
(4.14)

Note that this consequence is not limited to the specific initial density profiles (4.3) or (4.4).

Turning to Figs. 5(a) and 6(a), we see that the coincidence of the density contrast at $R/R_0\sim2.5$ ($R=R_c$) contributes to the accuracy of the Zel'dovich-type approximations, and δ_{ZA} and δ_{PZA} give a good fit around $R/R_0\sim2.5$. This is the reason that the Zel'dovich-type approximations do not necessarily give bad results even when the shell crossing is occurring.

V. SUMMARY AND DISCUSSIONS

We have tested the relativistic perturbative approximations to gravitational instability with the LTB solution. It has been shown that Zel'dovich-type approximations give higher accuracy than the conventional ones in the quasinonlinear regime $|\delta|\sim1$ within general relativistic framework. Our results are partly similar to the Newtonian ones, but our consideration is more generic. Especially, we considered some cases in which the matter distribution is inhomogeneous, and found that the Zel'dovich-type approximations are not necessarily inaccurate even when shell crossing occurs. Of course, the occurrence of the shell crossing shows the break down of our treatment. However, this is due to the failure of our description of the matter as dust rather than the failure of Zel'dovich-type approximations.

Indeed, one of the cases considered in the previous section includes the $f=0$ point, where the universe is locally ''open'' inside and is locally ''closed'' outside and shell crossing will occur at this radius. We have seen, in general, at the $f=0$ points (except the origin $R=0$), the deviation from the FLRW model is locally one dimensional and the

Zel'dovich-type approximations become exact. And in the neighborhood of the points, we can expect that the Zel'dovich-type approximations are particularly accurate. The case considered here is exactly such an example. It should be also noted that ''one dimensionality'' which makes the Zel'dovich-type approximations exact means not only globally plane symmetric but also locally one dimensional: Such situations appear even in the spherically symmetric model.

To discuss the applicable range of the Zel'dovich-type approximations, we reconsider the density contrast at $R=0$ in the collapse case. At the turnaround time, the accuracy of the Zel'dovich-type approximations already begins to fall down, i.e., δ_{PZA} is about 84% of δ_{LTB} and δ_{ZA} is about 60%. Inaccuracy will be accelerated beyond the turnaround time. In this sense, the turnaround epoch, when the peculiar velocity is as large as the Hubble expansion, is one of the criterion of the applicable range of the Zel'dovich-type approximations. However, this criterion might not be practical, because one cannot know the correct turnaround time in general, while we have been able to find it from the exact solution in our case. Instead of the turnaround time, the Zel'dovich-type approximations tell us the crunching time as the singularity in the density contrast, approximately. Furthermore, we have also seen that PZA tells us this crunching time more accurately than ZA in our spherical model. Then we may be able to know the approximate turnaround time by the half of this crunching time of PZA.

It is said that the Zel'dovich approximation predicts pancake formation in the gravitational collapse of dust [6]. But it is beyond the turnaround time that the pancake will be formed and thus the accuracy of the Zel'dovich approximation is not ensured at that time. If we try to examine the final stage of the collapse quantitatively, we will need to develop a new approximation scheme which gives an accurate description even beyond the turnaround epoch.

[1] P. J. E. Peebles, *The Large-Scale Structure of the Universe* (Princeton University Press, Princeton, 1980).

[2] E. M. Lifshitz, J. Phys. (Moscow) **10**, 116 (1946).

[3] W. H. Press and E. T. Vishniac, Astrophys. J. **239**, 1 (1980).

[4] J. M. Bardeen, Phys. Rev. D **22**, 1882 (1980); H. Kodama and M. Sasaki, Prog. Theor. Phys. Suppl. **78**, 1 (1984).

[5] K. Tomita, Prog. Theor. Phys. **37**, 831 (1967).

[6] Ya. B. Zel'dovich, Astron. Astrophys. **5**, 84 (1970).

[7] T. Buchert, Mon. Not. R. Astron. Soc. **254**, 729 (1992).

[8] T. Buchert and J. Ehlers, Mon. Not. R. Astron. Soc. **264**, 375 (1993).

[9] T. Buchert, Mon. Not. R. Astron. Soc. **267**, 811 (1994).

[10] F. R. Bouchet, S. Colombi, E. Hivon, and R. Juszkiewicz, Astron. Astrophys. **296**, 575 (1995).

[11] K. M. Croudace, J. Parry, D. S. Salopek, and J. M. Stewart, Astrophys. J. **423**, 22 (1994); D. S. Salopek, J. M. Stewart, and K. M. Croudace, Mon. Not. R. Astron. Soc. **271**, 1005 (1994).

[12] M. Kasai, Phys. Rev. D **52**, 5605 (1995).

[13] H. Russ, M. Morita, M. Kasai, and G. Börner, Phys. Rev. D **53**, 6881 (1996).

[14] S. Matarrese and D. Terranova, Mon. Not. R. Astron. Soc. **283**, 400 (1996).

[15] T. Buchert and G. Götz, J. Math. Phys. **28**, 2714 (1987); T. Buchert, Astron. Astrophys. **223**, 9 (1989).

[16] P. Szekeres, Commun. Math. Phys. **41**, 55 (1975).

[17] A. Krasiński, *Inhomogeneous Cosmological Models* (Cambridge University Press, Cambridge, England, 1997).

[18] D. Munshi, V. Sahni, and A. A. Starobinsky, Astrophys. J. **436**, 517 (1994).

[19] V. Sahni and S. Shandarin, Mon. Not. R. Astron. Soc. **282**, 641 (1996).

[20] V. Sahni and P. Coles, Phys. Rep. **262**, 1 (1995).

[21] A. Yoshisato, T. Matsubara, and M. Morikawa, Astrophys. J. (to be published).

[22] L. D. Landau and E. M. Lifshitz, *The Classical Theory of Fields* (Pergamon, Oxford, 1975).

[23] C. Hellaby and K. Lake, Astrophys. J. **290**, 381 (1985).

[24] M. Kasai, Phys. Rev. D **47**, 3214 (1993).